

## A HYBRID MULTI-OBJECT SEGMENTATION FRAMEWORK WITH MODEL-BASED B-SPLINES FOR MICROBIAL SINGLE CELL ANALYSIS

Karina Ruzaeva<sup>\*†</sup> Katharina Nöh<sup>\*</sup> Benjamin Berkels<sup>†</sup>

<sup>†</sup>AICES, RWTH Aachen University, Aachen, Germany

<sup>\*</sup>IBG-1: Biotechnology, Forschungszentrum Jülich GmbH, Jülich, Germany

### ABSTRACT

In this paper, we propose a hybrid approach for multi-object microbial cell segmentation. The approach combines an ML-based detection with a geometry-aware variational-based segmentation using B-splines that are parametrized based on a geometric model of the cell shape. The detection is done first using YOLOv5. In a second step, each detected cell is segmented individually. Thus, the segmentation only needs to be done on a per-cell basis, which makes it amenable to a variational approach that incorporates prior knowledge on the geometry. Here, the contour of the segmentation is modelled as closed uniform cubic B-spline, whose control points are parametrized using the known cell geometry. Compared to purely ML-based segmentation approaches, which need accurate segmentation maps as training data that are very laborious to produce, our method just needs bounding boxes as training data. Still, the proposed method performs on par with ML-based segmentation approaches usually used in this context. We study the performance of the proposed method on time-lapse microscopy data of *Corynebacterium glutamicum*.

**Index Terms**— B-Splines, microfluidic single cell analysis, cell segmentation

### 1. INTRODUCTION

Microfluidic single-cell analysis with time-lapse microscopy is a versatile tool to study cellular processes with spatio-temporal resolution. For instance, the analysis is used to reveal heterogeneity and cell dynamics in microbial populations with regard to growth, gene expression, cell interactions, production, or regulation [1, 2]. The possibility to generate large-scale datasets with automated time-lapse microscopy requires high-throughput single-cell feature extraction. To extract the features, each cell has to be segmented separately. Thus, robust, efficient and automatic multi-object segmentation for quantitative single-cell characterization is crucial [3].

Most traditional segmentation methods are general-purpose approaches and, thus, do not take prior knowledge on object geometry into account. In consequence, such methods may result in object geometries with unreasonable shapes. Going unnoticed, this may lead to biased results, in terms

of, e.g., cell area over time. In the case of state-of-the-art ML-based instance segmentation methods like Mask R-CNN [4], where object geometries can be learned implicitly, a large amount of training data is required. For microbial systems, benchmark data sets are lacking. One reason is that the creation of training data for segmentation is time-intensive and laborious. In particular, in the case of low-resolution and low-signal-to-noise ratio data, it is complicated to annotate images (draw cell outlines) even for domain experts.

Here, we use the biotechnologically relevant rod-shaped soil bacterium *Corynebacterium glutamicum* (*C. glutamicum*) [5, 6] as a model system to propose a solution for the notorious lack of ground truth (GT) data for microbial single cell analysis. In particular, our contribution to single cell image analysis is the development of a hybrid multi-object segmentation approach. Our approach is examined for *C. glutamicum* segmentation, and is summarized as follows. First, cells are detected based on the real-time detection framework YOLOv5 [7]. Second, each detected cell is segmented with a variational geometry-aware spline-based segmentation approach. Finally, the transferability of the segmentation approach to other non-rod-shaped bacteria with known geometries is demonstrated. A similar splitting into a detection step and a B-Spline-based segmentation step is introduced in [8]. The main benefits of the proposed approach are easy-to-create training datasets and that the segmentation preserves geometrical features for each segmentation instance by exploiting the available knowledge on cell morphology.

### 2. METHODS

We split multi-object segmentation into two steps. As first step, we use an ML-based detection approach. The main reason for separating the detection step is unlocking the variational segmentation method, which is otherwise infeasible due to the huge number of object instances to be segmented per image or region of interest [9]. Often, variational multi-object segmentation methods need laborious initialization and/or an interface for user interaction (e.g. manually drawing initial object outlines). Thus, automatic initialization for the subsequent segmentation step is very useful [10]. Another benefit of the two-stage process is reducing compu-

tational time and helping to avoid failed segmentation, caused by enclosing parts of nearby cells. Additionally, the detector is a useful fast cell counter that provides important process metrics for microfluidic experiments [11]. Another advantage of the splitting is that the segmentation can be done in parallel for the cells, since each detected bounding box contains only one full cell, which is then processed independently. Our source code is available on GitHub<sup>1</sup>.

## 2.1. Detection

As detection framework, we use YOLOv5, being the fastest detection framework available [7], whereas other choices are surely possible. The training and validation data was generated by the synthetic cell renderer CellSium<sup>2</sup>. In addition, a manually labeled real dataset was used. The overall training set size is 141 images, where 11 images are manually labeled.

## 2.2. Objective function

After the detection, each detected cell is segmented individually using a variational method. Variational methods formulate the given task, here, finding the cell border ( $\mathcal{C}$ ), as an optimization problem:  $\mathcal{C} = \arg \min_{\tilde{\mathcal{C}}} F(\tilde{\mathcal{C}})$

In our case, the idea is to define an objective function  $F$  that measures how well our conditions on the segmentation are fulfilled and apply optimization procedures to obtain an optimal segmentation of the central cell from the background (and parts of neighboring cells if present (Figure 1)) in the detection output. Specifically, the input are the image tiles, cropped according to the detected bounding boxes, where each image tile contains only one full cell, roughly centered in the tile and possibly parts of neighboring cells. Let  $I : \Omega \rightarrow \mathbb{R}$  denote the current image tile and  $\Omega \subset \mathbb{R}^2$  the corresponding image domain.

Our objective function  $F$  is the sum of three terms:

$$F(\mathcal{C}) = F_{\text{CE}}(\mathcal{C}) + w_R \cdot F_{\text{RE}}(\mathcal{C}) + w_D \cdot F_{\text{GE}}(\mathcal{C}) \quad (1)$$

Here, the terms are responsible for edge detection (contour-based term,  $F_{\text{CE}}$ ), for enclosing a region with given properties (region-based term,  $F_{\text{RE}}$ ), and for selectively enclosing a single object of interest (geodesic distance-based term,  $F_{\text{GE}}$ ). The selection of the weights  $w_R$ ,  $w_D$  is described in Section 3.

**Contour-based term** Object boundaries often coincide with edges in images, which are reflected by large image gradients [12, 10]. Hence, our objective  $F$  should maximize the average image gradient intensity along the contour. The corresponding term of the objective function, which encourages the contour to go through regions of high image gradient, is

$$F_{\text{CE}}(\mathcal{C}) = \frac{1}{\text{len}(\mathcal{C})} \int_{\mathcal{C}} \frac{1}{(|\nabla I(c)| + \varepsilon)^k} d\mathcal{H}^1(c). \quad (2)$$

<sup>1</sup>[https://github.com/kruzaeva/model\\_spline\\_seg](https://github.com/kruzaeva/model_spline_seg)

<sup>2</sup><https://github.com/modsim/CellSium>

Here,  $|\nabla I|$  is the norm of the image gradient (Figure 1c),  $\varepsilon = 0.001$  a regularization parameter to prevent division by zero,  $k = 1.5$  an empirically chosen power,  $\text{len}(\mathcal{C})$  the length of  $\mathcal{C}$  and  $\mathcal{H}^1$  the one-dimensional Hausdorff measure.

**Region-based term** In case of a crowded cell colony (cells touching each other),  $F_{\text{CE}}$  attracts the contour also to high-intensity gradient regions corresponding to the border of cells in the neighborhood of our target cell. To counter this undesired behavior, we use the additional term  $F_{\text{RE}}$ . Such a region energy encodes our prior knowledge on the image intensities. Since the image was recorded in bright field mode, cells have lower intensities than the surrounding background, minimization of the average intensity inside the contour is beneficial. The corresponding term in the objective function is

$$F_{\text{RE}}(\mathcal{C}) = \frac{1}{|\mathcal{R}(\mathcal{C})|} \int_{\mathcal{R}(\mathcal{C})} I(x, y) d(x, y) \quad (3)$$

Here,  $\mathcal{R}(\mathcal{C})$  denotes the region enclosed by  $\mathcal{C}$ .

**Geodesic distance term** Neither  $F_{\text{CE}}$  nor  $F_{\text{RE}}$  can distinguish the target cell in our current tile from neighboring cells that may also be visible in the tile. To account for this, we add a second region (geodesic distance) term, which aims to prevent the contour to enclose any point that would have to be connected to a marker  $M^T = [M_x, M_y]$  through a high gradient region [13]. Here, the marker needs to be inside the target cell and, to avoid user interaction, is chosen as the center of the bounding box. The geodesic distance map  $D$  (Figure 1d) is obtained with the geodesic distance transform by solving the Eikonal equation, implemented with raster scan, using the code from [14], with Figure 1(b) as an input and an empirically chosen image gradient weighting parameter = 0.8.

$$F_{\text{GE}}(\mathcal{C}) = \frac{1}{|\mathcal{R}(\mathcal{C})|} \int_{\mathcal{R}(\mathcal{C})} D(x, y) d(x, y) \quad (4)$$

Even though  $F_{\text{RE}}$  and the geodesic distance term  $F_{\text{GE}}$ , seem to be very similar, their combination improved the segmentation performance in our experiments.

Integrals over  $\mathcal{R}(\mathcal{C})$  can be rephrased using the divergence theorem as line integrals over  $\mathcal{C}$  [10]. Let  $\mathcal{R} \subset \mathbb{R}^2$  be a compact set with piecewise smooth boundary and  $\nu = (\nu_1, \nu_2)$  be the outer normal of  $\mathcal{R}$ . For  $f : \mathbb{R}^2 \rightarrow \mathbb{R}$  Lebesgue integrable, let  $f^x(x, y) = \int_0^x f(t, y) dt$  and  $f^y(x, y) = \int_0^y f(x, t) dt$ . Then, for  $F := \frac{1}{2}(f^x, f^y)$ , we get  $\text{div } F = f$  and thus

$$\int_{\mathcal{R}} f d(x, y) = \frac{1}{2} \int_{\partial \mathcal{R}} (f^x \nu_1 + f^y \nu_2) d\mathcal{H}^1(c). \quad (5)$$

Using (5), we rephrase  $F_{\text{RE}}$  and  $F_{\text{GE}}$  as integrals over  $\mathcal{C}$ .

## 2.3. Geometrical model

*C. glutamicum* cells can be represented with a simple geometrical model, i.e. as slightly bent rods. The contour  $\mathcal{C}$  is

represented as a closed cubic uniform B-Spline curve (for details we refer to [15]), as they, in the context of object segmentation, demonstrated solid performance in medical and biological data [10, 16, 17]. We propose to exploit the prior knowledge on the geometry by modeling the bent rod shape as closed B-spline curve with  $N = 6$  control points (cf. Figure 1), which is parametrized using 8 parameters: length segments ( $l_1$  and  $l_2$ ), width ( $w$ ), 2 curvature parameters ( $d$ ,  $e$ ), center ( $c_x$ ,  $c_y$ ), and rotation angle  $\alpha$ . Denoting the parameter vector by  $\theta = [c_x, c_y, l_1, l_2, w, d, e, \alpha]$ , the resulting coordinates of the six control points  $P(\theta) \in \mathbb{R}^{2 \times 6}$  are

$$P(\theta) = \begin{bmatrix} \cos \alpha & -\sin \alpha \\ \sin \alpha & -\cos \alpha \end{bmatrix} \cdot \begin{bmatrix} \tilde{P}_x(\theta) - c_x \\ \tilde{P}_y(\theta) - c_y \end{bmatrix} + \begin{bmatrix} c_x \\ c_y \end{bmatrix} \quad (6)$$

where

$$\begin{bmatrix} \tilde{P}_x(\theta) \\ \tilde{P}_y(\theta) \end{bmatrix} = \begin{bmatrix} \frac{w}{2}, \frac{w}{2} - d, -\frac{w}{2} - d, -\frac{w}{2}, -\frac{w}{2} - e, \frac{w}{2} - e \\ 0, l_1, l_1, 0, -l_2, -l_2 \end{bmatrix} \quad (7)$$

Note that the idea of parameterizing the geometry is not limited to bent rods, but applies to any kind of prior shape knowledge that can be expressed in terms of a parametrized spline (i.e. Figure 3d)). Such a geometric model-based approach provides target object features (i.e. lengths) with no need for post-processing to derive the target parameters from the obtained contour. Moreover, having geometric parameters as variables of an objective function, provides the possibility to apply shape constraints known from the application. In our case, these are biological constraints, such as limits on width  $w$  and height  $l_1 + l_2$  of the cells. Considering our rod model, we only expect minor deviations of target object features from the geometric parameters. As a result, the model parameters can be directly considered as target values.

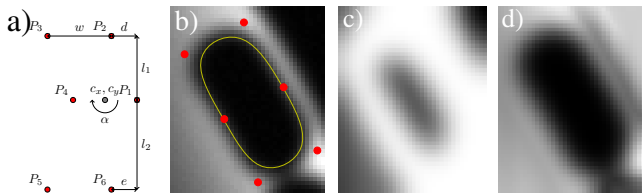


**Fig. 1.** Main components of the analysis: a) Geometrical model of *C. glutamicum* with  $P_i = (P(\theta)_{i1}, P(\theta)_{i2})$ , b) input of the objective  $F$  (cropped image tile  $I$  (output of the detection with the proposed model-based segmentation as overlay), c) gradient image  $\nabla I$  and d) geodesic distance map  $D$ ).

## 2.4. Preprocessing

To provide better segmentation results, as a preprocessing, we applied a set of simple image processing steps. To avoid undesired cropping of the parts of the cells, a 5 pixel padding was evenly applied for each bounding box. To unify the range

of pixel intensity values of each tile, the intensity image  $I$  in (3), the gradient image  $|\nabla I|$  in (2) and the geodesic distance map  $D$  in (4), were normalized to  $[0, 1]$ . Moreover, to prevent the attraction of the contour by high gradient regions in extracellular space and to prevent erroneous convergence to local minima, we applied Gaussian smoothing ( $\sigma = 3$ ) and clipping to  $|\nabla I|$  ( $[0, 0.45]$ ). This also reduces noise and the influence of undesired internal cell structures.

## 2.5. Minimization details

**Discretization** To evaluate the integrals over  $\mathcal{C}$ , an approximation of  $\mathcal{C}$  with a discrete curve is needed. To obtain a discrete curve, the contour is evaluated at a finite ( $n = 10$ ) number of equidistant parameter values per spline segment. The coordinates of a closed uniform B-spline for a given sequence of parameter values can be expressed as a matrix product of the spline control points coordinates  $P_{2 \times N}$  and the discrete spline coordinates matrix  $B_{N \times n \cdot N}(t)$ , where the matrix  $B$  is computed only once per experiment [15].

**Minimization method and constraints** As discussed in Section 2.3, the organism morphology dependent constraints can be directly applied to the variables of the objective function. According to [18], the segment lengths  $l_1, l_2$  are in the range of  $0.4\text{--}2\ \mu\text{m}$ . The overall length  $l = l_1 + l_2$  is constrained not to exceed the bounding box diagonal. The deviation from a straight rod in terms of  $d, e$  is limited to  $0.5\ \mu\text{m}$ . The expected width  $w$  of the cell is constrained to  $0.7\text{--}0.9\ \mu\text{m}$ . Considering the different ranges of the geometrical parameters ( $c_x, c_y, l_1, l_2, w, d, e$ ) and the rotation angle  $\alpha$ , the objective function  $F$  is minimized alternately using the ‘‘constrained optimization by linear approximation’’ (COBYLA) algorithm [19], implemented in [20]. This means, for a given number of iterations, the function  $F$  is minimized with respect to the geometrical parameters for a fixed angle, and analogously, with respect to the angle for fixed geometrical parameters.

**Initial Guess** The initialization may heavily influence the computed solution and the number of iterations, required to reach convergence. To minimize the number of failed segmentations due to undesired local minima, and number of iterations, the initial guess should be chosen carefully. We suggest considering a straight symmetrical ( $l_1 = l_2$ ) rod with proper orientation as initial guess. Orientation of the rod parameters was chosen considering the bounding box proportions: For a rectangular box (the length of the box exceeds its width by more than 20%), we use  $\alpha = 0^\circ$  or  $\alpha = 90^\circ$ , depending on which axis is longer. Otherwise, we use  $45^\circ$  or  $-45^\circ$ , depending on which angle results in a lower value of  $F_{GE}$  value. The initial rod parameters are:  $l_1 = l_2 = 0.5 \cdot \text{length of the greater dimension}$ ,  $w = 17$  pixels, since we have a  $0.065\ \mu\text{m}$  pixel size and expect our cells to be around  $1\ \mu\text{m}$  wide.

### 3. RESULTS

We evaluated the results of the proposed method using a validation dataset containing, due to the scarcity of real GT data, 30 synthetic (cf. Section 2.1) images with 2 to 196 cells.

**Detection results** The detection performance was evaluated using the mAP (mean average precision) score at IoU = 0.5 (intersection over union) and the mAP averaged over IoU = 0.5 : 0.95, cf. [21]. For the default Yolov5 parameters, NMS = 0.45 (empirically chosen non-maximum suppression parameter, which provides the highest mAP score) and Confidence = 0.6, we got: Average precision  $P = 1$ ; Average recall  $R = 0.98$ ;  $\text{mAP}_{0.5} = 0.97$ ;  $\text{mAP}_{0.5:0.95} = 0.76$ .

**Segmentation results** We used two metrics to evaluate the segmentation accuracy, based on the Dice score for binary segmentation. 1. *Foreground Dice score (FD)*, i.e. the dice score of a foreground mask. The cell colony is assumed as union of all single cell masks. Thus, the overlaps of cell masks are treated as belonging to the foreground once. 2. *Average multi-object Dice score (AMD)*, i.e. the average dice score for each single cell in comparison with the corresponding GT mask. Here, we check the segmentation accuracy, independently of the detection, using GT bounding boxes. The Dice scores of the proposed constrained geometry-aware method (GA+C) in the Table 1 is shown against the non-constrained geometry-aware method (GA) and a conventional (non-parametrized) spline fit (nGA), with the same number of control points. For the latter, the objective (1) was minimized with respect to control points coordinates.

The weights  $w_R$ ,  $w_D$  were chosen using [22] with  $1 - \text{AMD}(w_R, w_D)$  as objective function, assuming that  $w_R$  and  $w_D$  are uniformly distributed in  $[0, 500]$  with the number of optimization attempts = 1000. The objective function was calculated using frame 15 of the validation set sequence, which contains 15 cells. Figure 2 illustrates, that despite a non-

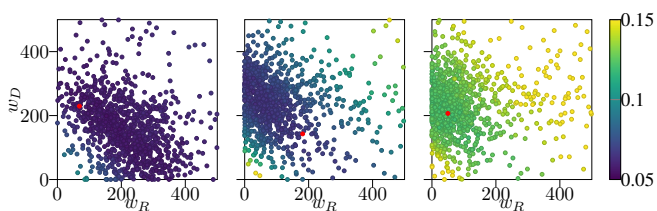


**Fig. 2.** Weight optimization results. Left to right: geometry-aware segmentation with constraints, without constraints and unconstrained segmentation with control points as variables. The red point shows the best result for each method.

significant gain in terms of accuracy (cf. Table 1), the constrained geometry-aware segmentation method shows visible improvement in terms of robustness, i.e. model insensitivity to the objective function’s weights choice.

**Table 1.** Segmentation scores. An example GA+C result and the respective ground truth is depicted in Figure 3a,b

Image (number of cells)	FD			AMD		
	GA+C	GA	nGA	GA+C	GA	nGA
1(2)	0.9471	0.9041	0.8982	0.9471	0.9038	0.8978
5(3)	0.9356	0.9253	0.6719	0.9445	0.9317	0.7385
10(7)	0.9420	0.9391	0.8232	0.9447	0.9405	0.8491
15(15)	0.9451	0.9413	0.8835	0.9460	0.9421	0.8826
20(32)	0.9377	0.9373	0.7036	0.9366	0.9350	0.6375
25(71)	0.9408	0.9386	0.6647	0.9393	0.9355	0.6647
30(196)	0.9329	0.9297	0.8070	0.9297	0.9260	0.8134

The average FD score of the proposed (GA+C) segmentation method, based on the YOLO bounding boxes, for the 30 images, is 0.86. Unfortunately, a direct comparison with literature results of the state-of-the-art algorithms is not possible since no benchmark data sets with our target microorganism are available. The available numbers indicate that the proposed method outperforms U-net and EDNN based segmentation, trained and tested with comparable amount of real instead of synthetic images [23] (0.63 and 0.79, respectively) and is on par with Mask RCNN trained with synthetic data generated by CellSium and tested with real data, in terms of Dice score, applied to a *C. glutamicum* dataset. Moreover, the proposed method significantly decreases the manual labor for training data creation, since only bounding boxes need to be provided instead of pixel-precise segmentation masks.

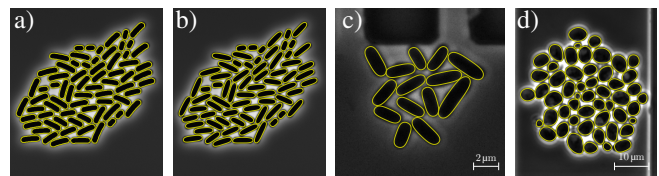


**Fig. 3.** a) Ground truth (GT) data and the result of the proposed method applied to b) the GT artificial image, c) real *C. glutamicum* data based on a rod-shape model (Section 2.3), d) the *S. cerevisiae* based on the ovoid-shape model.

### 4. CONCLUSIONS

We proposed a hybrid approach, combining ML-based detection with variational model-based segmentation. Given the robustness of the approach and easy-to-create training data, we expect it to be an effective framework for other image segmentation tasks in microfluidic single-cell analysis. The approach is not only limited to rod-shaped cells (Figure 3c), there are many organisms with known geometries that can be modelled using simple geometrical models. Another example of such an organism is *Saccharomyces cerevisiae*. *S. cerevisiae* cells are round to ovoid, 5–10  $\mu\text{m}$  diameter [24] and can be represented similarly, as a parametrized closed spline with 6 control points. The result of the geometry-aware segmentation of *S. cerevisiae* is illustrated in Figure 3d).

## 5. COMPLIANCE WITH ETHICAL STANDARDS

Ethical approval is not applicable because this work does not contain any studies with animal or human subjects.

## 6. ACKNOWLEDGMENTS

This work was performed as part of the Helmholtz School for Data Science in Life, Earth and Energy (HDS-LEE) and received funding from the Helmholtz Association.

## References

- [1] Christian Dusny and Alexander Grünberger, “Microfluidic single-cell analysis in biotechnology: from monitoring towards understanding,” *Current Opinion in Biotechnology*, vol. 63, pp. 26–33, June 2020.
- [2] Vera Ortseifen et al., “Microfluidics for Biotechnology: Bridging Gaps to Foster Microfluidic Applications,” *Frontiers in Bioengineering and Biotechnology*, vol. 8, 2020.
- [3] Markus Leygeber et al., “Analyzing Microbial Population Heterogeneity—Expanding the Toolbox of Microfluidic Single-Cell Cultivations,” *Journal of Molecular Biology*, vol. 431, no. 23, pp. 4569–4588, 2019.
- [4] Kaiming He et al., “Mask R-CNN,” in *2017 IEEE ICCV*. Oct. 2017, IEEE.
- [5] Lothar Eggeling and Michael Bott, Eds., *Handbook of Corynebacterium glutamicum*, CRC Press, Mar. 2005.
- [6] Kei-Anne Baritugo et al., “Metabolic engineering of *Corynebacterium glutamicum* for fermentative production of chemicals in biorefinery,” *Applied Microbiology and Biotechnology*, vol. 102, no. 9, pp. 3915–3937, 2018.
- [7] Glenn Jocher et al., “ultralytics/yolov5: v5.0 - yolov5-p6 1280 models, aws, supervise.ly and youtube integrations,” 2021.
- [8] Soham Mandal and Virginie Uhlmann, “Splinedist: Automated cell segmentation with spline curves,” in *2021 IEEE 18th International Symposium on Biomedical Imaging (ISBI)*. Apr. 2021, IEEE.
- [9] Yan Nei Law et al., “A variational model for segmentation of overlapping objects with additive intensity value,” *IEEE Transactions on Image Processing*, vol. 20, no. 6, pp. 1495–1503, June 2011.
- [10] R. Delgado-Gonzalo and M. Unser, “Spline-based framework for interactive segmentation in biomedical imaging,” *IRBM*, vol. 34, no. 3, pp. 235–243, June 2013.
- [11] Alexander Grünberger et al., “Beyond growth rate 0.6:corynebacterium glutamicumcultivated in highly diluted environments,” *Biotechnology and Bioengineering*, vol. 110, no. 1, pp. 220–228, Aug. 2012.
- [12] R. Delgado-Gonzalo et al., “Snakes with an ellipse-reproducing property,” *IEEE Transactions on Image Processing*, vol. 21, no. 3, pp. 1258–1271, Mar. 2012.
- [13] Michael Roberts, Ke Chen, and Klaus L. Irion, “A convex geodesic selective model for image segmentation,” *Journal of Mathematical Imaging and Vision*, vol. 61, no. 4, pp. 482–503, Nov. 2018.
- [14] Guotai Wang et al., “DeepIGeoS: A deep interactive geodesic framework for medical image segmentation,” *IEEE Transactions on Pattern Analysis and Machine Intelligence*, vol. 41, no. 7, pp. 1559–1572, July 2019.
- [15] Carl de Boor, *A Practical Guide to Splines*, Springer-Verlag GmbH, 2001.
- [16] P. Brigger et al., “B-spline snakes: a flexible tool for parametric contour detection,” *IEEE Transactions on Image Processing*, vol. 9, no. 9, pp. 1484–1496, 2000.
- [17] Soham Mandal and Virginie Uhlmann, “A learning-based formulation of parametric curve fitting for bioimage analysis,” Tech. Rep., bioRxiv, Jan. 2020.
- [18] Joris Messelink et al., “Single-cell growth inference of corynebacterium glutamicum reveals asymptotically linear growth,” *bioRxiv*, May 2020.
- [19] M. J. D. Powell, “Direct search algorithms for optimization calculations,” *Acta Numerica*, vol. 7, pp. 287–336, Jan. 1998.
- [20] Pauli Virtanen et al., “SciPy 1.0: Fundamental Algorithms for Scientific Computing in Python,” *Nature Methods*, vol. 17, pp. 261–272, 2020.
- [21] Sean Bell et al., “Inside-outside net: Detecting objects in context with skip pooling and recurrent neural networks,” in *Proceedings of the IEEE Conference on CVPR*, June 2016.
- [22] James Bergstra et al., “Making a science of model search: Hyperparameter optimization in hundreds of dimensions for vision architectures,” in *Proceedings of the 30th ICML 2013, Atlanta, GA, USA, 16-21 June 2013*. 2013, vol. 28 of *JMLR Workshop and Conference Proceedings*, pp. 115–123, JMLR.org.
- [23] Christian Carsten Sachs, *Online high throughput microfluidic single cell analysis for feed-back experimentation*, Dissertation, RWTH Aachen University, 2018.
- [24] Horst Feldmann, *Yeast : molecular and cell biology*, Wiley-VCH, Weinheim, 2010.